JACS
JOURNAL OF THE AMERICAN CHEMICAL SOCIETY
Article
pubs.acs.org/JACS

All Solution-Processed Lead Halide Perovskite-$BiVO_4$ Tandem Assembly for Photolytic Solar Fuels Production

Yong-Siou Chen,[†,‡,∥] Joseph S. Manser,[†,§,∥] and Prashant V. Kamat*[,†,‡,§]

[†]Radiation Laboratory, University of Notre Dame, Notre Dame, Indiana 46556, United States
[‡]Department of Chemistry and Biochemistry, University of Notre Dame, Notre Dame, Indiana 46556, United States
[§]Department of Chemical and Biomolecular Engineering, University of Notre Dame, Notre Dame, Indiana 46556, United States

Supporting Information

ABSTRACT: The quest for economic, large-scale hydrogen production has motivated the search for new materials and device designs capable of splitting water using only energy from the sun. Here we introduce an all solution-processed tandem water splitting assembly composed of a $BiVO_4$ photoanode and a single-junction $CH_3NH_3PbI_3$ hybrid perovskite solar cell. This unique configuration allows efficient solar photon management, with the metal oxide photoanode selectively harvesting high energy visible photons, and the underlying perovskite solar cell capturing lower energy visible-near IR wavelengths in a single-pass excitation. Operating without external bias under standard AM 1.5G illumination, the photoanode−photovoltaic architecture, in conjunction with an earth-abundant cobalt phosphate catalyst, exhibits a solar-to-hydrogen conversion efficiency of 2.5% at neutral pH. The design of low-cost tandem water splitting assemblies employing single-junction hybrid perovskite materials establishes a potentially promising new frontier for solar water splitting research.

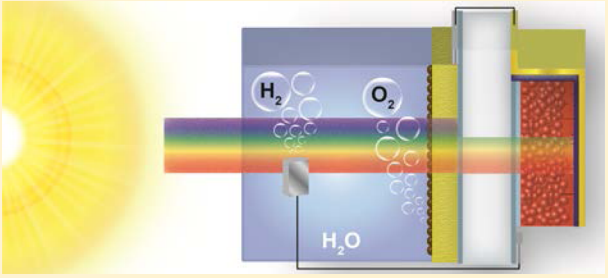

INTRODUCTION

Practical implementation of large-scale solar-based renewable energy resources requires efficient conversion and storage of photons across the visible spectrum. Taking inspiration from the natural photosynthetic process, conversion of light into chemical energy provides a convenient route to store the abundant yet intermittent solar photon flux for on-demand and remote use. In this regard, one of the most promising approaches involves the generation of hydrogen gas from visible-light driven water splitting.[1−3] It has been suggested that hydrogen will be a ubiquitous fuel of the future due to its high specific energy (J/kg) and environmentally benign byproducts in fuel cell applications.[4]

Meeting the thermodynamic requirements for solar water splitting (1.23 V at standard temperature and pressure) and the associated overpotential necessary to drive water oxidation and reduction has led to a variety of creative combinations of light-harvesting and electrocatalytic assemblies.[5−11] The ideal photolytic (or photocatalytic) water splitting system, with direct interfacial contact between light-absorber and aqueous solution, would be composed of a single, visibly active semiconductor with suitable band alignment to drive hydrogen and oxygen production. Certain wide band gap metal oxides such as $SrTiO_3$ can perform unassisted water photolysis, but are only active under near-UV irradiation,[12,13] severely limiting their viability in single-material systems. The requirement for increased visible absorption has driven the development of numerous n-type semiconductor metal oxides including bismuth vanadate ($BiVO_4$),[14] tungsten oxide (WO_3),[15] and hematite (α-Fe_2O_3)[16] due to their relatively low band gaps and effective operation as photoanodes for water oxidation. With a band gap of ∼2.4 eV (∼520 nm) and high conduction band energy relative to other visibly active metal oxides, $BiVO_4$ is an especially promising photoanode material.[10,17−20] However, photogenerated electrons in $BiVO_4$ are not sufficiently energetic to induce unassisted proton reduction. Researchers have therefore turned to multiple absorber schemes known as "D4" systems (D − dual absorber, 4 − minimum number of absorbed photons to generate one H_2 molecule) to circumvent the practical issues associated with single absorber models. One such D4 architecture consists of a $BiVO_4$ photoanode coupled to a second light-absorber (photocathode or photovoltaic device) that can effectively boost electron energy and drive the water reduction half reaction.[10,20,21] In addition to favorable band edge alignment, the two correlated light-harvesting elements must exhibit complementary spectral sensitivity to maximize solar-to-hydrogen (STH) conversion efficiency in single-pass tandem device operation.[22] This design is analogous to the photosynthetic Z-scheme and can enable bias-free solar water splitting using a wide array of material combinations.[23,24]

Until now, efficient tandem photoanode−photovoltaic (PV) water splitting designs using $BiVO_4$ have included a single or multijunction silicon solar cell to provide additional energy for

Received: November 21, 2014
Published: December 27, 2014

DOI: 10.1021/ja511739y
J. Am. Chem. Soc. 2015, 137, 974−981

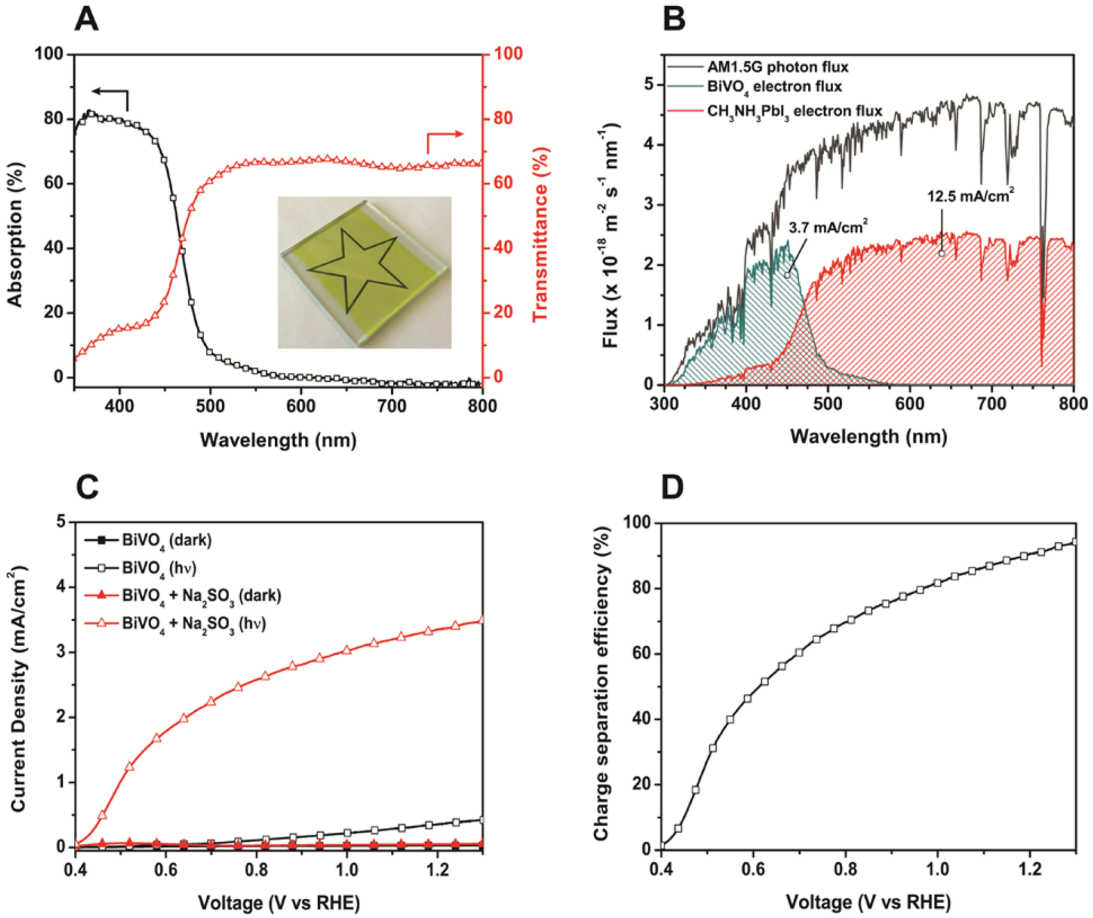

Figure 1. Optical and photoelectrochemical characterization of the $BiVO_4$ photoanode. (A) Optical absorption and transmittance of the $BiVO_4$ thin film. Inset: photograph demonstrating the translucence and limited visible light scattering of the spin-cast $BiVO_4$ thin film. (B) Predicted electron flux at the $BiVO_4$ photoanode and $CH_3NH_3PbI_3$ PV calculated by integrating the $BiVO_4$ absorption and transmittance across the AM 1.5G solar spectrum, assuming 100% internal quantum efficiency and 80% external quantum efficiency for $BiVO_4$ and $CH_3NH_3PbI_3$, respectively. (C) Photoelectrochemical characteristics of the $BiVO_4$ photoanode in 0.5 M aqueous Na_2SO_4 with and without 0.5 M Na_2SO_3 as a sacrificial reagent. The anodic current response signifies the n-type nature of $BiVO_4$. Photoanode area was 0.15 cm^2. (D) Charge separation efficiency of $BiVO_4$, specifying the fraction of photogenerated charges that reach the semiconductor−electrolyte interface as a function of applied bias.

unassisted water splitting.[10,20] These stand-alone devices have recently demonstrated maximum STH efficiency of 5.2% using a dual junction amorphous silicon/nanocrystalline silicon (*a*-Si/nc-Si) solar cell.[20] This is the highest reported efficiency for a metal oxide photoanode, evincing the promise of $BiVO_4$ for water oxidation. Considering the facile solution processing of $BiVO_4$ photoanodes by spin or spray deposition, energy intensive construction of the coupled multijunction solar cell remains the primary fabrication bottleneck in these tandem systems.

Our present objective is to strike a balance between $BiVO_4$−PV device complexity and photolytic performance, bearing in mind that the practical viability of such systems can be enhanced by reducing material and fabrication costs. Supplanting silicon-based PVs in tandem water splitting architectures requires a unique material that is amenable to simple, low-cost processing yet yields high photovoltaic output across the visible spectrum. Promising solid-state compounds known as "hybrid" organic−inorganic lead halide perovskites have recently emerged as exceptional materials for next-generation photovoltaic technologies.[25,26] These compounds can be processed from solution near ambient conditions while simultaneously exhibiting excellent semiconducting properties,[27−29] providing a low-cost, highly efficient substitute to silicon-based devices. Perovskite solar cell efficiencies have already surpassed much more mature DSSCs and organic photovoltaics in a few short years of development.[30,31] The low band gap and large absorption coefficient of lead iodide hybrid perovskites facilitate effective thin film light harvesting into the near-IR region of the solar spectrum.[32] Rapid improvement in perovskite solar cell power conversion efficiency and, most notably for photolytic applications, extremely high photovoltage in comparison to nearly all other single-junction PV technologies,[25] warrant exploration into the feasibility of this material in tandem water splitting architectures. As recently demonstrated, two series-connected perovskite solar cells externally wired to submerged electrocatalysts can provide sufficient voltage to drive water splitting in an electrolytic configuration.[33] In the same regard, a synergistic paring of the most efficient emerging PV technology[34] with the champion metal oxide photoanode material[20] is a promising route in the quest for inexpensive solar fuels production. Toward this goal, we report a tandem, bias-free, fully solution-processed water splitting system based on a $BiVO_4$ photoanode and a single-junction methylammonium lead triiodide ($CH_3NH_3PbI_3$) perovskite solar cell. The hybrid photoanode-PV design has an added benefit of spatially

DOI: 10.1021/ja511739y
J. Am. Chem. Soc. 2015, 137, 974−981

isolating the moisture-sensitive perovskite cell from the aqueous environment. We demonstrate that the $CH_3NH_3PbI_3$ PV provides complementary absorption and the requisite energy to drive hydrogen and oxygen production when coupled to $BiVO_4$ in a photolytic D4 architecture.

RESULTS AND DISCUSSION

$BiVO_4$ Photoanode Optical and Photoelectrochemical Behavior. The use of $BiVO_4$ in photolytic water splitting systems is fundamentally different than electrolytic designs employing isolated light-harvesting and electrocatalytic components. For solar (PV)-driven electrolysis, energy supplied to the electrodes is derived from multijunction or series-connected photovoltaic devices.[2] In the case of *a*-Si solar cells, three or more devices must be connected in series to generate the necessary potential for water splitting.[6] Conversely, photolytic schemes require one or more light-harvesting semiconductor components to be direct contact with water. With respect to PV-induced electrolysis, the benefits of solar photolysis are fourfold: (i) reduction in balance-of-systems costs due to the potential for monolithically integrated components,[2] (ii) equilibration of energy levels near the semiconductor-electrolyte interface establishes a built-in potential for driving charge flow,[2] (iii) injection of minority rather than majority carriers into solution raises the maximum obtainable electron−hole energy,[35] and (iv) restriction of current density to the area of the semiconductor thin film mitigates additional overpotential associated with larger current densities in commercial electrolyzers.[36] These key distinctions between electrolytic and photolytic systems stimulated our investigation into the capabilities of a $BiVO_4$-hybrid perovskite photolytic architecture.

In designing tandem photoanode−PV devices, the optical density of the top layer must be carefully tuned to allow sufficient transmission of light to the subsequent absorber material. It is therefore essential to characterize and tailor photoanode extinction. $BiVO_4$ thin films were deposited on fluorine doped tin oxide (FTO) optically transparent electrodes via spin coating of a mixed solution of bismuth nitrate ($Bi(NO_3)_3{\cdot}9H_2O$) and vanadyl acetylacetonate ($VO(acac)_2$) precursors, followed by annealing at 500 °C (full experimental details in the Supporting Information). The as-prepared photoanode films exhibited X-ray diffraction patterns characteristic of monoclinic $BiVO_4$ (Supporting Information Figure S1).[37,38] Figure 1A shows the optical extinction properties of the spin-cast $BiVO_4$ layer. The absorption percentage of the yellow-colored photoanode (after correcting for scattering effects) reaches ∼80% at 400 nm, corresponding to a film thickness of ∼240 nm assuming an absorption coefficient of 3×10^4 cm^{-1} at 400 nm.[39] While the absorption characteristics determine the maximum possible photocurrent that can be generated by the $BiVO_4$ photoanode, the transmitted light denotes the photon energies that reach the underlying PV. With a transmittance of nearly 70% at wavelengths greater than 500 nm, the $BiVO_4$ film displays little to no scattering considering the FTO electrode alone accounts for ∼20% loss in transmittance across the visible spectrum (Supporting Information Figure S2).

A salient feature of $BiVO_4$ photoanodes is the ability to generate high photocurrent densities with relatively flat, unstructured films, which dramatically reduces optical scattering and simplifies the fabrication process.[10] The scanning electron micrograph of the $BiVO_4$ surface in Supporting Information Figure S3 reveals the compact and homogeneous nature of the spin-cast photoanode. Although nanostructuring can improve the performance of metal oxide electrodes due to shortened carrier diffusion requirements,[19] their efficacy in tandem architectures can be hindered by high levels of scattering at energies below the band gap.[40] In addition, nanostructured thin films tend to require more complicated fabrication methods and are more difficult to optically tune. In contrast, the optical attenuation of the spin-cast planar films can be precisely controlled by simply tailoring the number of coating cycles. These features render the high-transmittance $BiVO_4$ films presented here well suited to accommodate a secondary absorber material in a low-cost, solution-processed tandem device.

On the basis of the absorbance and transmittance of the $BiVO_4$ photoanode, it is possible to determine the upper bound performance of both semiconductor components in the tandem light-harvesting assembly. This analysis is depicted in Figure 1B. Integrating the $BiVO_4$ absorbance across the Air Mass 1.5 Global (AM 1.5G) solar spectrum, and assuming an internal quantum efficiency of unity, yields the maximum obtainable electron flux at the photoanode. This flux corresponds to a current density of 3.7 mA/cm^2. Because the $BiVO_4$ layer acts as a filter for the solar irradiance impinging on the underlying $CH_3NH_3PbI_3$ PV, integrating the transmittance of the photoanode provides a realistic estimation of the maximum photocurrent output of the perovskite solar cell in the tandem architecture. Assuming an external quantum efficiency of 80% at wavelengths below 800 nm corresponds to an upper bound short-circuit current density of 12.5 mA/cm^2. This excellent photocurrent output highlights the limited scattering losses at the $BiVO_4$ photoanode and the complementary absorption between $BiVO_4$ and $CH_3NH_3PbI_3$. It is clear from Figure 1B that the tandem device should display strong broadband light absorption from the UV into the near-IR region of the solar spectrum.

Following optical characterization of the $BiVO_4$ thin film, the photoelectrochemical performance of the photoanode was investigated using a three electrode configuration consisting of a Pt counter and Ag/AgCl reference electrode (three electrode experimental parameters detailed in the Supporting Information). The anodic current density−voltage ($J-V$) curves in Figure 1C illustrate the n-type semiconductor nature of bare $BiVO_4$ in the presence and absence of 0.5 M sodium sulfite (Na_2SO_3). Here, Na_2SO_3 acts a sacrificial hole scavenger whose oxidation is more energetically and kinetically facile relative to water oxidation.[19] The low photocurrent density (0.38 mA/cm^2 at 1.23 V vs reversible hydrogen electrode (RHE)) and high-bias current onset (∼0.5 V vs RHE) without Na_2SO_3 are indicative of the sluggish water oxidation kinetics and large overpotential on bare $BiVO_4$. Addition of Na_2SO_3 results in nearly an order of magnitude enhancement in photocurrent density at 1.23 V vs RHE and cathodically shifted onset potential, clearly reflecting more favorable interfacial hole transfer processes to the sacrificial donor. This increased performance represents an upper bound for photoanode current output in absence of the complex rate-determining water oxidation reaction.

Photoelectrochemical testing in the presence of Na_2SO_3 enables isolation of the intrinsic charge separation processes in the $BiVO_4$ electrode. The measured photocurrent that passes through the external circuit is a function of several parameters and can be characterized by the expression[19,41]

DOI: 10.1021/ja511739y
J. Am. Chem. Soc. 2015, 137, 974−981

$$J_{PEC} = J_{abs} \times \eta_{sep} \times \eta_{cat} \quad (1)$$

where J_{PEC} is the current density obtained from the $J-V$ measurement with Na_2SO_3, J_{abs} is the current density derived from the optical absorbance assuming 100% internal quantum efficiency (3.7 mA/cm^2), η_{sep} is the fraction of photogenerated holes that reach the semiconductor−electrolyte interface, and η_{cat} is the fraction of those holes that are injected into solution for sulfite oxidation. Because of the rapid oxidation kinetics of Na_2SO_3, we assume $\eta_{cat} \approx 1$, allowing for determination of η_{sep} using eq 1. The charge separation efficiency is plotted as a function of applied potential in Figure 1D. The separation efficiency of the intrinsic $BiVO_4$ film approaches 90% at 1.23 V vs RHE, indicating a large majority of the photogenerated holes eventually reach the semiconductor surface. Despite the low carrier mobility in intrinsic $BiVO_4$, the hole diffusion length (~70 nm) outpaces other photocatalytically relevant metal oxides such as Fe_2O_3 (~4 nm) and CuO_2 (~25 nm) as a result of long carrier lifetimes,[17] facilitating the use of planar $BiVO_4$ films in photolytic applications.

$CH_3NH_3PbI_3$ Photovoltaic Performance. Previous ultraviolet photoelectron spectroscopy measurements indicate the valence and conduction band edges of $CH_3NH_3PbI_3$ are suitably positioned for unassisted water splitting at neutral pH.[42] With single-junction $CH_3NH_3PbI_3$ solar cells producing voltages above 1.2 V,[43] solar hydrogen generation using a single perovskite device is within the realm of possibility. However, thermodynamic limitations restrict the maximum open circuit potential of $CH_3NH_3PbI_3$ (E_g = 1.5 eV) to ~1.3 V at room temperature.[44] Even with today's state-of-the-art hydrogen and oxygen evolution catalysts, this upper bound photovoltage for a single-junction $CH_3NH_3PbI_3$ device is not sufficient to account for overpotential associated with the water splitting reaction. Luo and co-workers recently employed two high-efficiency $CH_3NH_3PbI_3$ solar cells connected in a side-by-side series configuration to carry out water splitting in a conventional electrolyzer with submerged catalyst electrodes.[33] While advancements in low-cost solar electrolyzers are important for realization of widespread H_2 generation, photolytic systems have several distinct advantages (vide supra) that continue to motivate substantial research investment since their first demonstration four decades ago.[45]

The solution-processed perovskite solar cell was fabricated by two-step deposition of $CH_3NH_3PbI_3$ onto mesoporous TiO_2. The spiro-OMeTAD (2,2′,7,7′-tetrakis(*N*,*N*-di-*p*-methoxyphenylamine)-9,9′-spirobifluorene) hole transport material was layered on top of the $TiO_2/CH_3NH_3PbI_3$ thin film, followed by evaporation of a gold counter electrode (see Supporting Information for full solar cell fabrication methods). A characteristic $J-V$ curve of the $CH_3NH_3PbI_3$ solar cell is shown in Figure 2. Under AM 1.5G illumination, the perovskite solar cell exhibited a power conversion efficiency of 13.4%. The integrated photocurrent obtained from the external quantum efficiency (18.8 mA/cm^2) correlates well with the measured short-circuit current density (J_{SC}) of 19.1 mA/cm^2 (Supporting Information Figure S4). An open-circuit voltage (V_{OC}) of 1.03 V is indicative of the low-loss nature of this system ($V_{OC.Obs}/V_{OC.Theor.}$ = 0.79). The high voltage from this single-junction device, in combination with a large fill factor (0.68), bodes well for $CH_3NH_3PbI_3$ solar cell operation in a photoanode−PV system.

To simulate the tandem configuration, the same solar cell was tested with a $BiVO_4$ thin film placed in front of the light source. The $BiVO_4$ window acts as a long pass filter blocking out the majority of light below ~500 nm, resulting in nearly 50% reduction of power density compared to one sun conditions (51 mW/cm^2). The $J-V$ curve in Figure 2 demonstrates the exceptional performance of the $CH_3NH_3PbI_3$ solar cell under this modified illumination. Despite excluding nearly all high energy visible and UV photons, the J_{SC} remained approximately half of the one sun value. Most notably, we detected no measurable decrease in open-circuit potential, and the increased fill factor (0.71) resulted in an improved power conversion efficiency of 15.5%. Since the voltage and fill factor of the underlying solar cell in a photoanode-PV system have profound impact on the overall device performance,[46] the constancy of these parameters in the presence of $BiVO_4$ is vital for efficient tandem solar fuels generation.

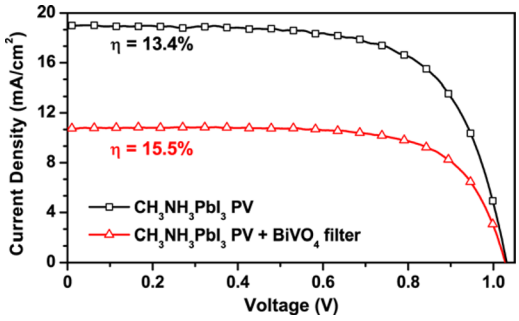

Figure 2. Photocurrent density−voltage characteristics of the $CH_3NH_3PbI_3$ solar cell. Under one sun illumination, the $CH_3NH_3PbI_3$ solar cell operated at 13.4% efficiency. A $BiVO_4$ film served as a filter to determine the performance of the underlying solar cell in a tandem configuration. Under these modified irradiation conditions, corresponding to an intensity of 51 mW/cm^2, the same solar cell exhibited an increased efficiency of 15.5% owing to an improved fill factor and sustained open-circuit voltage. Device area was 0.12 cm^2.

$BiVO_4$−$CH_3NH_3PbI_3$ Tandem Device. In assembling the photoanode−PV device, the two light-harvesting modules were arranged in a layered fashion and connected in series. A scheme depicting the $BiVO_4$−$CH_3NH_3PbI_3$ architecture is illustrated in Figure 3 (a photograph of the operating device is shown in Supporting Information Figure S5), depicting the transmission of wavelengths >500 nm through the $BiVO_4$ photoanode. Complementary spectral sensitivity of each component in the tandem assembly facilitates selective harvesting of photons in a single-pass excitation. This photon management strategy enables a higher photovoltage output than could be realized through the operation of either individual component. Two different aqueous solutions were employed in the operation of the tandem device. The first set of experiments employed Na_2SO_3 as a sacrificial donor, facilitating direct examination of the water reduction capabilities of the single-junction perovskite PV when coupled to $BiVO_4$. The second set of experiments consisted of 0.1 M phosphate buffered aqueous solution (pH 7) which enabled testing of the tandem device's ability to drive complete water splitting. The relevant oxidative reactions that occur at the photoanode in each solution are defined in Figure 3.

To determine the spectral response of the tandem architecture, we measured the external quantum efficiency (EQE) of each light absorbing component (Figure 4A), providing a measure of the fraction of incident photons at a given wavelength converted to extractable charges. The EQE of the $CH_3NH_3PbI_3$ PV was measured through a $BiVO_4$ filter to

DOI: 10.1021/ja511739y
J. Am. Chem. Soc. 2015, 137, 974−981

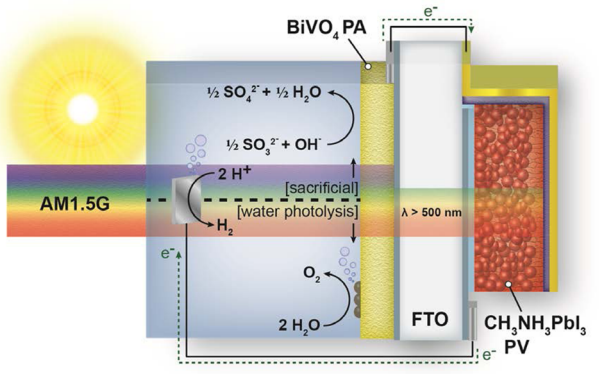

Figure 3. Schematic diagram of the tandem $BiVO_4$–$CH_3NH_3PbI_3$ device for solar fuels generation. The two different systems (sacrificial and water photolysis) depict the oxidative reactions at the $BiVO_4$ photoanode in the presence and absence of the sacrificial donor Na_2SO_3. In both cases, the perovskite solar cell harnesses transmitted photons above 500 nm, and the resulting photogenerated electrons drive H_2 production. A cobalt–phosphate catalyst was utilized to alleviate the sluggish $BiVO_4$ water oxidation kinetics in the full water splitting system.

simulate tandem operation. The panchromatic response of the photoanode–PV system is immediately apparent, with a minimum EQE of ~40% between 350 and 760 nm. The shape of $CH_3NH_3PbI_3$ PV EQE spectrum correlates well with transmission through the $BiVO_4$ photoanode (see Figure 1A), confirming that higher energy visible photons are harvested by $BiVO_4$ and lower energy visible and near-IR wavelengths are efficiently captured by the $CH_3NH_3PbI_3$ solar cell. The combination of solution-processed $BiVO_4$ and $CH_3NH_3PbI_3$ provides excellent photoresponse to greater than 50% of the solar radiation that reaches earth's surface.

Because of the series connection between the two modules, the operating photocurrent density of a tandem photoanode-PV device can be predicted from the intersection of the individual *J*–*V* curves. This reflects the fact that photogenerated electrons in $BiVO_4$ recombine with holes in $CH_3NH_3PbI_3$, requiring that the current flowing through each module be equivalent. The approximate band energies of the various components in the tandem assembly, as well as the expected interfacial charge transfer processes that describe current flow between the photoanode and PV components, are shown in Supporting Information Figure S6. From the crossing point of the superimposed *J*–*V* curves in Figure 4B, we expect a photocurrent density of ~1.9 mA/cm^2 with approximately 80% charge separation efficiency in the $BiVO_4$ electrode (Figure 1D) when employing the Na_2SO_3 sacrificial donor, provided

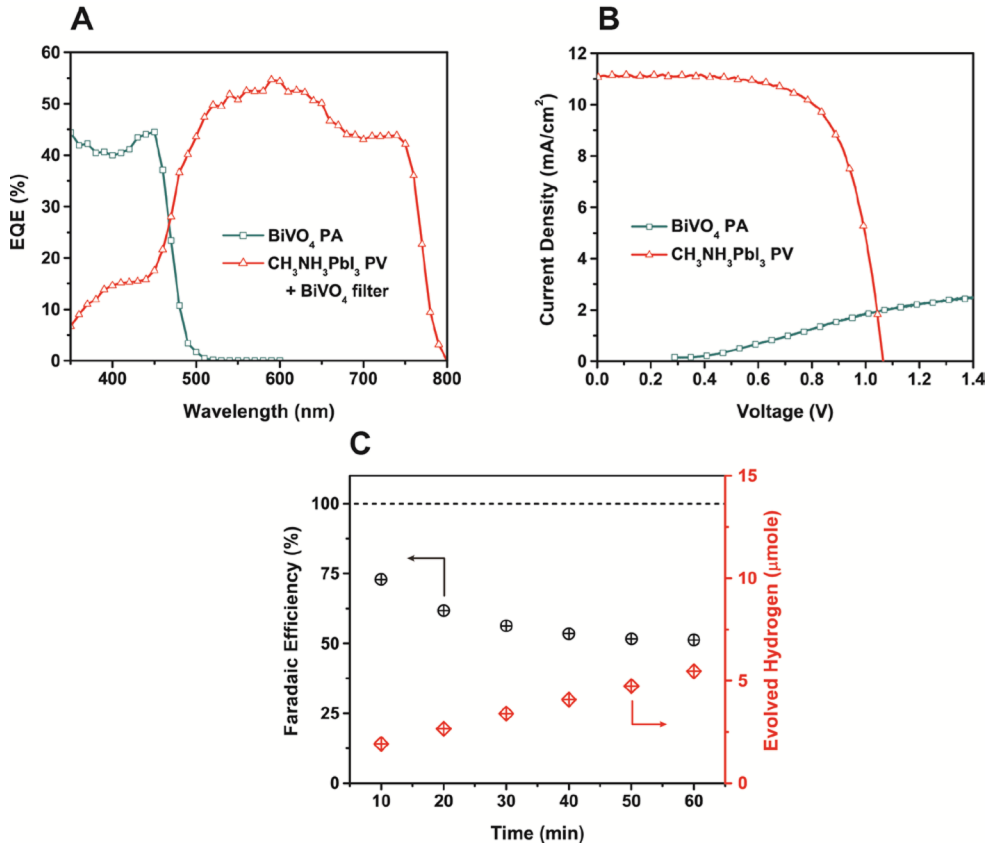

Figure 4. Solar hydrogen generation utilizing tandem $BiVO_4$–$CH_3NH_3PbI_3$ and sacrificial reagent. All $BiVO_4$ and tandem device measurements were carried out in a mixed aqueous solution of 0.5 M Na_2SO_4 and 0.5 M Na_2SO_3 (pH 9.3) with a photoactive area of 0.54 cm^2. (A) External quantum efficiency (EQE) of the individual $BiVO_4$ photoanode and $CH_3NH_3PbI_3$ PV. $BiVO_4$ EQE was recorded at 1 V bias vs a Pt counter electrode. The perovskite solar cell EQE was measured through a $BiVO_4$ filter. (B) Superimposed *J*–*V* curves of the individual $BiVO_4$ and $CH_3NH_3PbI_3$ components. The $BiVO_4$ photoelectrochemical properties were measured in a two electrode setup with a Pt counter electrode. The predicted operating point of the tandem device is at the intersection of the two curves. (C) Faradaic efficiency and quantity of detected hydrogen derived from the $BiVO_4$–$CH_3NH_3PbI_3$ tandem assembly under standard one sun AM 1.5G irradiation.

DOI: 10.1021/ja511739y
J. Am. Chem. Soc. 2015, 137, 974–981

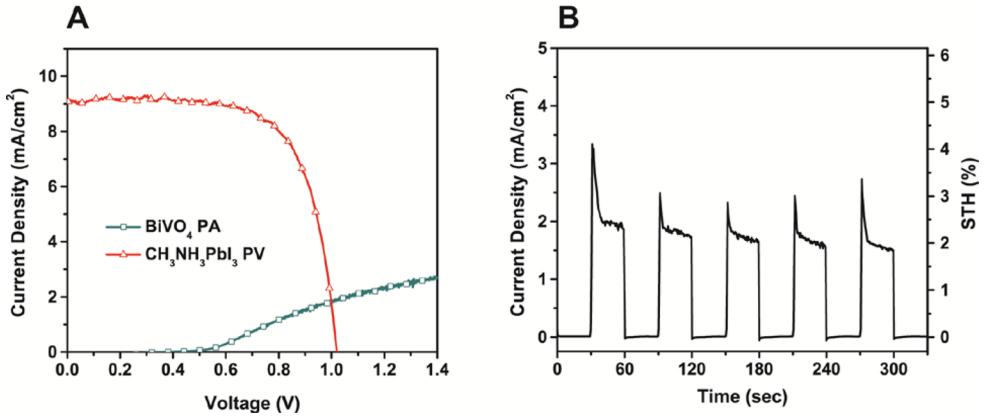

Figure 5. CoPi/$BiVO_4$–$CH_3NH_3PbI_3$ solar water splitting. All $BiVO_4$ and tandem measurements were performed in 0.1 M aqueous phosphate solution (pH 7) with a photoactive area of 0.15 cm^2. (A) Overlay of the *J*–*V* characteristics of CoPi/$BiVO_4$ photoanode and $CH_3NH_3PbI_3$ solar cell. The photovoltaic parameters were recorded through a CoPi/$BiVO_4$ film. CoPi/$BiVO_4$ was measured in a three electrode configuration with Ag/AgCl reference and Pt counter electrodes. The crossing point of the two curves designates the anticipated photocurrent output of the series-connected tandem assembly. (B) Photocurrent density and calculated solar-to-hydrogen conversion (STH) efficiency as a function of time for the CoPi/$BiVO_4$–$CH_3NH_3PbI_3$ device, demonstrating the ability to drive neutral water oxidation and reduction at 2.5% efficiency without external bias.

electrons in $CH_3NH_3PbI_3$ are energetic enough to reduce water at the submerged Pt electrode.

The photocurrent output of the $BiVO_4$–$CH_3NH_3PbI_3$ tandem device over 1 h of constant AM 1.5G illumination is shown in Supporting Information Figure S7. The corresponding Faradaic efficiency and quantity of evolved H_2 gas (as measured by gas chromatography) are given in Figure 4C. The amount of charge that passed through the tandem device is presented in Supporting Information Figure S8. Initially, the current density matched closely with the anticipated value (~1.75 mA/cm^2), indicating that electrons derived from the perovskite solar cell can indeed induce proton reduction at the Pt surface. Following the initial response, photocurrent output declined and eventually stabilized after approximately 10 min of H_2 production. Upon investigation of this instability, we found that neither the perovskite solar cell nor the $BiVO_4$ photoanode exhibited significant signs of degradation. Instead, the decrease in performance manifested from deleterious reactions between the Pt electrode and products of sacrificial reagent oxidation. A thorough explanation of this conclusion is provided in the Supporting Information and in Figures S9–S13. Despite instabilities at the Pt electrode, we observed significant H_2 evolution from the tandem configuration (Supporting Information Movie S1). This encouraging result confirms the hybrid perovskite PV is capable of driving hydrogen generation in this tandem architecture.

Following realization of proficient H_2 production with $CH_3NH_3PbI_3$, the next logical step was to test the full water splitting capabilities of tandem $BiVO_4$–$CH_3NH_3PbI_3$. To overcome kinetic barriers of water oxidation at the photoanode, cobalt phosphate (CoPi) was photodeposited onto $BiVO_4$. CoPi is a widely used earth-abundant oxygen evolution catalyst (OEC),[47] preserving the low-cost, solution-processed nature of the $BiVO_4$ and $CH_3NH_3PbI_3$ components in the tandem device. The photocurrent measured upon illumination of $BiVO_4$ (biased at 0.3 V vs Ag/AgCl) in a solution of 0.05 mM Co^{2+} and 0.1 M phosphate is shown in Supporting Information Figure S14. The anodic response reflects oxidation of solution-based Co^{2+} to solid Co^{3+} on the electrode surface.[48] A representative scanning electron micrograph of the CoPi/$BiVO_4$ surface in Supporting Information Figure S15 reveals the thin layer of photodeposited catalyst.

The three electrode *J*–*V* characteristics of CoPi/$BiVO_4$ in Supporting Information Figure S16 demonstrate the excellent activity of the catalyst toward water oxidation. The photoanode employing CoPi shows nearly a 4-fold enhancement in current density compared to bare $BiVO_4$ at 1 V vs RHE. A peak EQE of ~55% at 450 nm further corroborates the high turnover frequency afforded by the CoPi catalyst (Supporting Information Figure S17). The degree of visible light absorption by CoPi OEC had to be carefully controlled considering the photoanode is subjected to front side illumination in the tandem water splitting architecture (the light passes first through $BiVO_4$ before reaching the optically transparent electrode). The high EQE confirms that the CoPi layer employed here provides adequate surface coverage without significantly hindering light absorption by the underlying $BiVO_4$.

Current density–voltage characteristics of CoPi/$BiVO_4$ shown in Figure 5A were measured in a neutral pH three electrode configuration. We expect similar photoanode output in the tandem device as evidenced by the identical performance of CoPi/$BiVO_4$ in H_2-saturated two electrode and N_2-saturated three electrode measurements (Supporting Information Figure S18). With the high photocurrent densities achieved in the tandem system, Nernstian shifts due to changes in dissolved H_2 concentration near the Pt electrode are negligible.[10] Figure 5A shows the anticipated operating point of the CoPi/$BiVO_4$–$CH_3NH_3PbI_3$ water splitting device, specified by the intersection between the *J*–*V* curves of the two individual semiconductor components. From this point we expect a photocurrent output of approximately 2 mA/cm^2.

The performance of the tandem device in 0.1 M phosphate solution (pH 7) is displayed in Figure 5B. Photocurrent response in absence of sacrificial compounds verifies that CoPi/$BiVO_4$–$CH_3NH_3PbI_3$ can indeed produce sufficient energy for unassisted solar fuels generation. Taking the Faradaic efficiency (η_F) as unity[49] and using the thermodynamic potential for water splitting (1.23 V), we can determine the unassisted STH efficiency (η_{STH}) according to eq 2.[9]

DOI: 10.1021/ja511739y
J. Am. Chem. Soc. 2015, 137, 974–981

$$\eta_{STH}(\%) = \frac{J_{PEC} \times 1.23 \times \eta_F}{P_{IN}} \times 100 \quad (2)$$

Here, J_{PEC} is the measured photocurrent density (in mA/cm^2) and P_{IN} is the power density of the incident photon flux (100 mW/cm^2 at standard AM 1.5G conditions). The photocurrent generated under AM 1.5G illumination corresponds to a STH efficiency of 2.5% for the CoPi/$BiVO_4$–$CH_3NH_3PbI_3$ tandem device (Figure 5B). We posit that the initial photocurrent transient upon illumination stems from excess charges in the perovskite solar cell that must equilibrate with the current generated in the $BiVO_4$ photoanode. The slight decline in photocurrent over the course of the water splitting reaction is attributed to partial dissolution of the CoPi catalyst.[21] Other earth-abundant OECs (e.g., FeOOH and NiOOH) have been shown to exhibit improved stability at neutral pH, enabling constant photolytic water oxidation over 45 h of continuous operation.[19] Utilization of such materials in the OEC/$BiVO_4$–$CH_3NH_3PbI_3$ water splitting system could potentially mitigate these issues.

CONCLUDING REMARKS

Though substantial optimization remains, the CoPi/$BiVO_4$–$CH_3NH_3PbI_3$ water splitting capabilities are among the highest for solution-processed tandem architectures reported to date,[9] and are comparable to efficiencies obtained using wireless triple-junction *a*-Si electrolyzers.[6] Dramatically reduced device complexity afforded by the single-junction $CH_3NH_3PbI_3$ PV provides a competitive alternative to more expensive technologies in $BiVO_4$ tandem water splitting applications. The all solution-processed device exhibits relatively small discrepancy in performance compared to the most efficient $BiVO_4$-single-junction PV systems that employ complex gradient-doped photoanodes and *a*-Si components.[10,20] It should be noted that while the series connection between the photoanode and PV components used here enabled screening of the capabilities of this tandem configuration, monolithic designs incorporating internal graded recombination layers can potentially reduce resistive and optical losses stemming from the FTO electrodes, further boosting photolytic output. However, from the current setup it is clear that utilization of inexpensive materials, fabrication methods, and earth-abundant OECs make the CoPi/$BiVO_4$–$CH_3NH_3PbI_3$ architecture a new gateway to low-cost solar hydrogen production.

Demonstrating single-junction hybrid perovskite functionality in tandem water splitting applications establishes a foundation for exploring various low-cost photoanode-perovskite PV combinations. The sustained photovoltage and photoconversion efficiency of the single-junction $CH_3NH_3PbI_3$ PV even under low energy excitation enables exceptional performance in tandem light-harvesting assemblies. The operating point of the CoPi/$BiVO_4$–$CH_3NH_3PbI_3$ PV device is well below the solar-to-electricity conversion efficiency of the underlying perovskite solar cell, stemming from the limited photocurrent density of the $BiVO_4$ photoanode. Therefore, significant opportunities exist for advancing metal oxide photoanode capabilities when used in conjunction with perovskite solar cells. Improving the $BiVO_4$ absorption and light-harvesting efficiency while maintaining limited scattering at longer wavelengths could markedly enhance $BiVO_4$-perovskite PV output. With all other parameters remaining fixed in the CoPi/$BiVO_4$–$CH_3NH_3PbI_3$ system investigated herein, realizing only ∼60% of the maximum theoretical photocurrent of $BiVO_4$ would yield a STH efficiency over 5%. Alternatively, coupling single-junction perovskite solar cells to lower band gap metal oxides with sufficiently negative flat band potentials could equalize the absorbed photon flux between the two layers, providing better utilization of the full capabilities of the perovskite PV.[22] Replacing $CH_3NH_3^+$ cations with larger formamidinium ions ($HC(NH_2)_2^+$) opens possibilities for lowering the band gap, bathochromically shifting the absorption onset and enhancing lead halide perovskite functionality as an underlying layer in tandem light harvesting assemblies.[50,51]

ASSOCIATED CONTENT

Supporting Information

Experimental section, supporting text, Figures S1–S18, Movie S1. This material is available free of charge via the Internet at http://pubs.acs.org.

AUTHOR INFORMATION

Corresponding Author

pkamat@nd.edu

Author Contributions

‖These authors contributed equally.

Notes

The authors declare no competing financial interest.

ACKNOWLEDGMENTS

The authors would like to thank Professor Nam-Gyu Park and Dae-Yong Son for offering their expertise on perovskite solar cell fabrication. Partial support was provided by the Center for Sustainable Energy at Notre Dame (cSEND) and the Notre Dame Integrated Imaging Facility. The research described herein was supported by the Division of Chemical Sciences, Geosciences, and Biosciences, Office of Basic Energy Sciences of the U.S. Department of Energy, through award DE-FC02-04ER15533. This is contribution number NDRL No. 5051 from the Notre Dame Radiation Laboratory.

REFERENCES

(1) Bard, A. J.; Fox, M. A. *Acc. Chem. Res.* **1995**, *28*, 141.
(2) Walter, M. G.; Warren, E. L.; Mckone, J. R.; Boettcher, S. W.; Mi, Q.; Santori, E. A.; Lewis, N. S. *Chem. Rev.* **2010**, *110*, 6446.
(3) Tachibana, Y.; Vayssieres, L.; Durrant, J. R. *Nat. Photonics* **2012**, *6*, 511.
(4) Turner, J. A. *Science* **1999**, *285*, 687.
(5) Chen, Y.-S.; Kamat, P. V. *J. Am. Chem. Soc.* **2014**, *136*, 6075.
(6) Reece, S. Y.; Hamel, J. A.; Sung, K.; Jarvi, T. D.; Esswein, A. J.; Pijpers, J. J. H.; Nocera, D. G. *Science* **2011**, *334*, 645.
(7) Khaselev, O. *Science* **1998**, *280*, 425.
(8) Hou, Y.; Abrams, B. L.; Vesborg, P. C. K.; Björketun, M. E.; Herbst, K.; Bech, L.; Setti, A. M.; Damsgaard, C. D.; Pedersen, T.; Hansen, O.; Rossmeisl, J.; Dahl, S.; Nørskov, J. K.; Chorkendorff, I. *Nat. Mater.* **2011**, *10*, 434.
(9) Brillet, J.; Yum, J.; Cornuz, M.; Hisatomi, T.; Solarska, R.; Augustynski, J.; Graetzel, M.; Sivula, K. *Nat. Photonics* **2012**, *6*, 824.
(10) Abdi, F. F.; Han, L.; Smets, A. H. M.; Zeman, M.; Dam, B.; van de Krol, R. *Nat. Commun.* **2013**, *4*, 2195.
(11) Liu, C.; Tang, J.; Chen, H. M.; Liu, B.; Yang, P. *Nano Lett.* **2013**, *13*, 2989.
(12) Mavroides, J. G.; Kafalas, J. A.; Kolesar, D. F. *Appl. Phys. Lett.* **1976**, *28*, 241.
(13) Townsend, T. K.; Browning, N. D.; Osterloh, F. E. *ACS Nano* **2012**, *6*, 7420.
(14) Park, Y.; McDonald, K. J.; Choi, K.-S. *Chem. Soc. Rev.* **2013**, *42*, 2321.

DOI: 10.1021/ja511739y
J. Am. Chem. Soc. 2015, 137, 974–981

(15) Bignozzi, C. A.; Caramori, S.; Cristino, V.; Argazzi, R.; Meda, L.; Tacca, A. *Chem. Soc. Rev.* **2013**, *42*, 2228.
(16) Sivula, K.; Le Formal, F.; Grätzel, M. *ChemSusChem* **2011**, *4*, 432.
(17) Abdi, F. F.; Savenije, T. J.; May, M. M.; Dam, B.; van de Krol, R. *J. Phys. Chem. Lett.* **2013**, *4*, 2752.
(18) Lichterman, M. F.; Shaner, M. R.; Handler, S. G.; Brunschwig, B. S.; Gray, H. B.; Lewis, N. S.; Spurgeon, J. M. *J. Phys. Chem. Lett.* **2013**, *4*, 4188.
(19) Kim, T. W.; Choi, K.-S. *Science* **2014**, *343*, 990.
(20) Han, L.; Abdi, F. F.; van de Krol, R.; Liu, R.; Huang, Z.; Lewerenz, H.-J.; Dam, B.; Zeman, M.; Smets, A. H. M. *ChemSusChem* **2014**, *7*, 2832.
(21) Bornoz, P.; Abdi, F. F.; Tilley, S. D.; Dam, B.; van de Krol, R.; Graetzel, M.; Sivula, K. *J. Phys. Chem. C* **2014**, *118*, 16959.
(22) Bolton, J. R.; Strickler, S. J.; Connolly, J. S. *Nature* **1985**, *316*, 495.
(23) Sasaki, Y.; Kato, H.; Kudo, A. *J. Am. Chem. Soc.* **2013**, *135*, 5441.
(24) Maeda, K.; Abe, R.; Domen, K. *J. Phys. Chem. C* **2011**, *115*, 3057.
(25) Snaith, H. J. *J. Phys. Chem. Lett.* **2013**, *4*, 3623.
(26) Park, N. *J. Phys. Chem. Lett.* **2013**, *4*, 2423.
(27) Manser, J. S.; Kamat, P. V. *Nat. Photonics* **2014**, *8*, 737.
(28) Wehrenfennig, C.; Eperon, G. E.; Johnston, M. B.; Snaith, H. J.; Herz, L. M. *Adv. Mater.* **2014**, *26*, 1584.
(29) Stamplecoskie, K. G.; Manser, J. S.; Kamat, P. V. *Energy Environ. Sci.* **2014**, *8*, 208.
(30) Hodes, G. *Science* **2013**, *342*, 317.
(31) Kamat, P. V.; Christians, J. A.; Radich, J. G. *Langmuir* **2014**, *30*, 5716.
(32) Xing, G.; Mathews, N.; Sun, S.; Lim, S. S.; Lam, Y. M.; Gratzel, M.; Mhaisalkar, S.; Sum, T. C. *Science* **2013**, *342*, 344.
(33) Luo, J.; Im, J.-H.; Mayer, M. T.; Schreier, M.; Nazeeruddin, M. K.; Park, N.-G.; Tilley, S. D.; Fan, H. J.; Gratzel, M. *Science* **2014**, *345*, 1593.
(34) Best Research-Cells Efficiencies. http://www.nrel.gov/ncpv/images/efficiency_chart.jpg.
(35) Nozik, A. J. *Appl. Phys. Lett.* **1977**, *30*, 567.
(36) Turner, J.; Sverdrup, G.; Mann, M. K.; Maness, P.; Kroposki, B.; Ghirardi, M.; Evans, R. J.; Blake, D. *Int. J. Energy Res.* **2008**, *32*, 379.
(37) Jeong, H. W.; Jeon, T. H.; Jang, J. S.; Choi, W.; Park, H. *J. Phys. Chem. C* **2013**, *117*, 9104.
(38) Rettie, A. J. E.; Lee, H. C.; Marshall, L. G.; Lin, J.-F.; Capan, C.; Lindemuth, J.; McCloy, J. S.; Zhou, J.; Bard, A. J.; Mullins, C. B. *J. Am. Chem. Soc.* **2013**, *135*, 11389.
(39) Zhao, Z.; Li, Z.; Zou, Z. *Phys. Chem. Chem. Phys.* **2011**, *13*, 4746.
(40) Brillet, J.; Cornuz, M.; Formal, F. Le; Yum, J.-H.; Grätzel, M.; Sivula, K. *J. Mater. Res.* **2011**, *25*, 17.
(41) Zhou, M.; Bao, J.; Bi, W.; Zeng, Y.; Zhu, R.; Tao, M.; Xie, Y. *ChemSusChem* **2012**, *5*, 1420.
(42) Schulz, P.; Edri, E.; Kirmayer, S.; Hodes, G.; Cahen, D.; Kahn, A. *Energy Environ. Sci.* **2014**, *7*, 1377.
(43) Ishii, A.; Jena, A. K.; Miyasaka, T. *APL Mater.* **2014**, *2*, 091102.
(44) Shockley, W.; Queisser, H. J. *J. Appl. Phys.* **1961**, *32*, 510.
(45) Fujishima, A.; Honda, K. *Nature* **1972**, *238*, 37.
(46) Prévot, M. S.; Sivula, K. *J. Phys. Chem. C* **2013**, *117*, 17879.
(47) Kanan, M. W.; Nocera, D. G. *Science* **2008**, *321*, 1072.
(48) Kanan, M. W.; Surendranath, Y.; Nocera, D. G. *Chem. Soc. Rev.* **2009**, *38*, 109.
(49) Zhong, D. K.; Choi, S.; Gamelin, D. R. *J. Am. Chem. Soc.* **2011**, *133*, 18370.
(50) Koh, T. M.; Fu, K.; Fang, Y.; Chen, S.; Sum, T. C.; Mathews, N.; Mhaisalkar, S. G.; Boix, P. P.; Baikie, T. *J. Phys. Chem. C* **2014**, *118*, 16458.
(51) Eperon, G. E.; Stranks, S. D.; Menelaou, C.; Johnston, M. B.; Herz, L. M.; Snaith, H. J. *Energy Environ. Sci.* **2014**, *7*, 982.

DOI: 10.1021/ja511739y
J. Am. Chem. Soc. 2015, 137, 974−981